Supplementary Information

Engineering Diamond-Based Photocathodes for Visible Light-Driven Hydrogen Generation

Alessandro Bellucci[1,], Davide Barreca[2], Chiara Maccato[2,3], Ermanno Pierobon[3], Gian Andrea Rizzi[3], Gaetana Petrone[4,5], Andrea Liscio[4], Leonardo Mattiello[5], Eleonora Bolli[1], Matteo Mastellone[1], Raffaella Salerno[1,6], Riccardo Polini[6], Veronica Valentini[1], Daniele M. Trucchi[1]*

[*]*alessandro.bellucci@cnr.it*

Table of contents

1. Electrochemical test setup

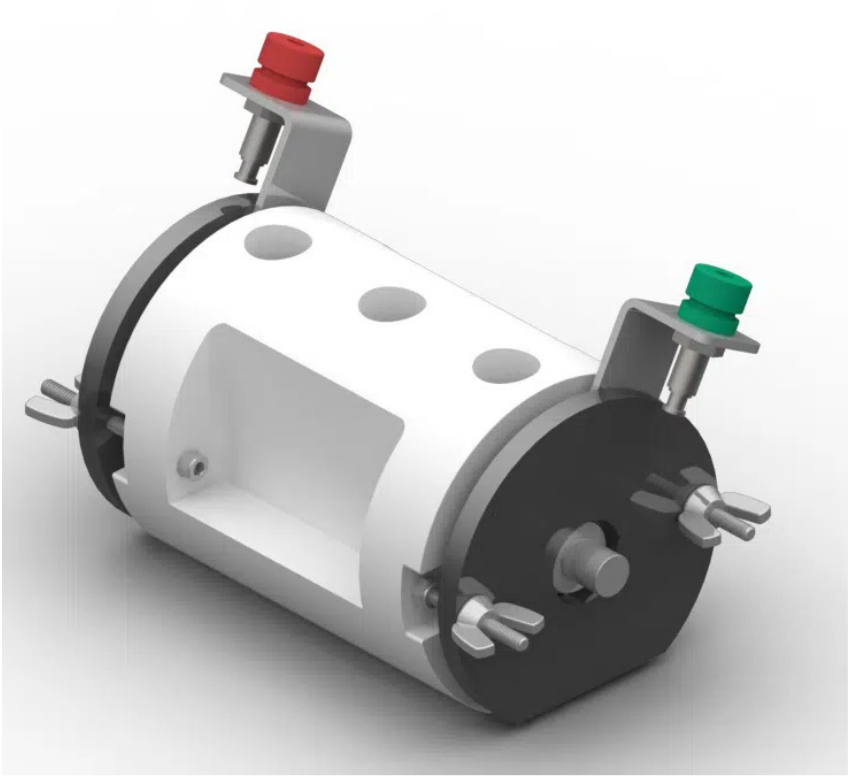

Figure S1. *Schematic representation of the cell used to perform electrochemical tests (PINE Research; overall volume = 45 mL). The samples were mounted outside the cell and kept in position by an O-ring seal. All samples were illuminated from the front side through a quartz window.*

2. Field emission-scanning electron microscopy (FE-SEM)

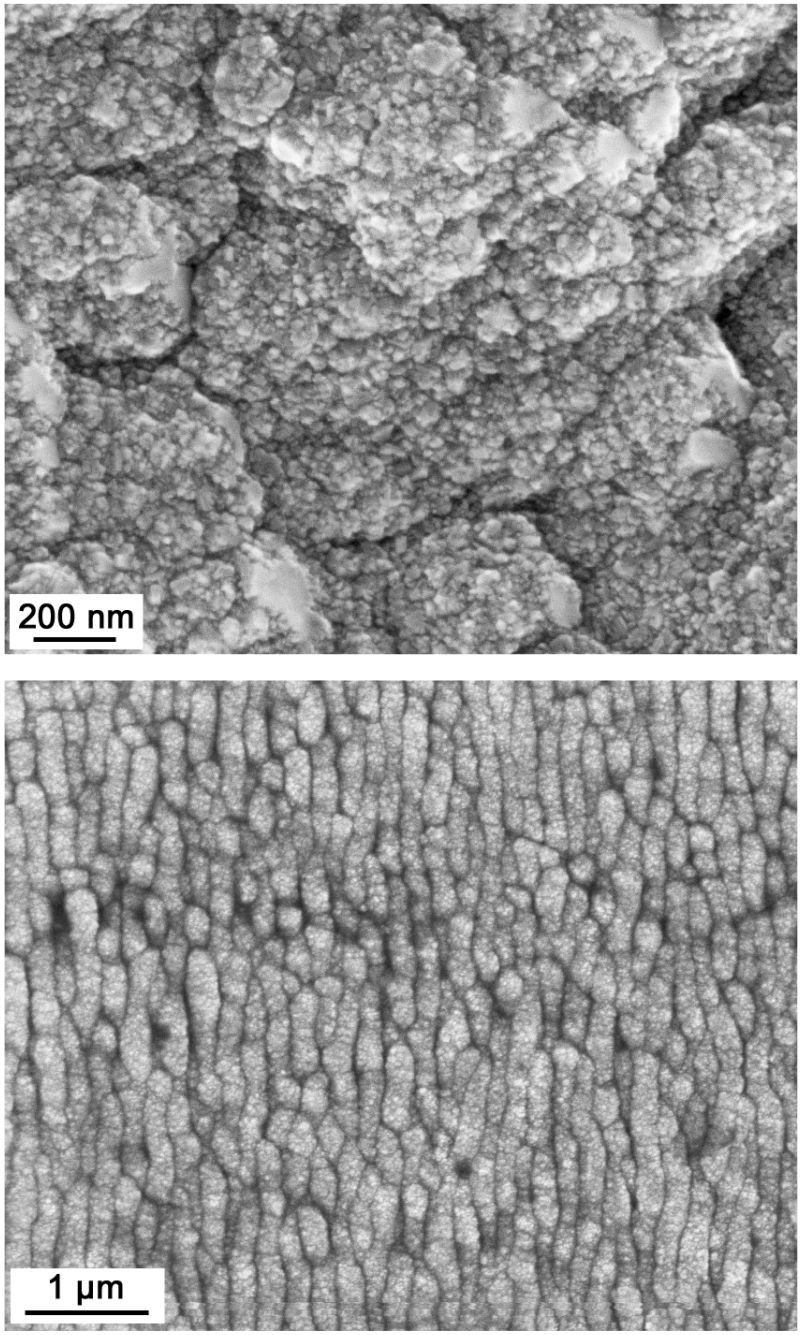

Figure S2. *Representative FE-SEM micrographs of the N-incorporated UNCD film (upper panel) and black diamond (BD) layer (lower panel), both produced starting from a commercial polycrystalline diamond plate.*

3. Atomic force microscopy (AFM)

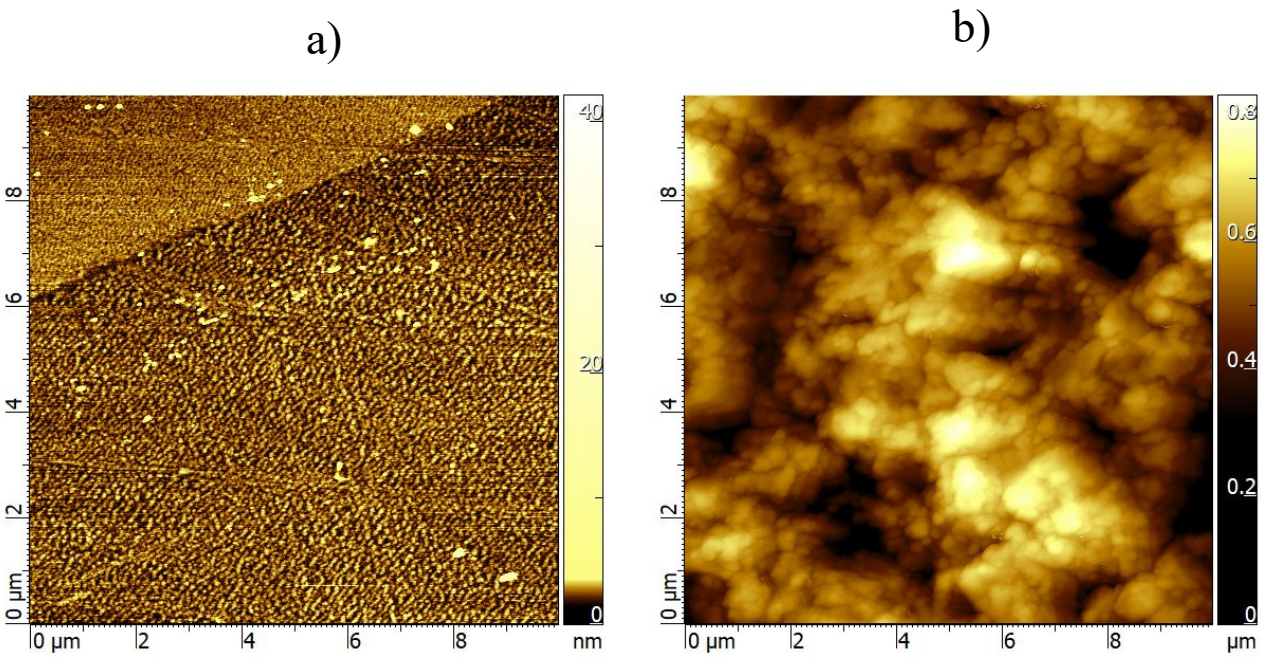

Figure S3. *AFM micrographs of: a) polished surface of the pristine plate; b) lapped (opaque) surface of the pristine plate. The root-mean-square (RMS) roughness is (0.7 ± 0.1) nm for the polished surface and (97 ± 1) nm for the lapped surface.*

4. X-ray photoelectron spectroscopy (XPS)

Table S1. *Atomic percentages (at.%) for the specimens under investigation before electrochemical tests.*

Sample	C (at.%)	O (at.%)	N (at.%)
BD-N-UNCD	98.7	1.3	---
BD-N-UNCD-H	94.4	4.8	0.8

Table S2. *XPS results: binding energy (BE) and contributions (%) of the various bands for the overall C1s, O1s and N1s peaks before electrochemical tests.*

Sample	C_1		C_2		C_3	
	BE (C_1) (eV)	% (C_1)	BE (C_2) (eV)	% (C_2)	BE (C_3) (eV)	% (C_3)
BD-N-UNCD	285.0	94.2	286.2	5.8	---	---
BD-N-UNCD-H	285.0	71.1	286.1	20.6	289.2	8.3
Sample	**O_1**		**O_2**		**O_3**	
	BE (O_2) (eV)	% (O_2)	BE (O_3) (eV)	% (O_3)	BE (O_4) (eV)	% (O_4)
BD-N-UNCD	531.5	19.3	532.6	57.3	533.8	23.4
BD-N-UNCD-H	531.6	7.6	532.5	45.7	533.8	46.7
Sample	**N_1**		**N_2**		**N_3**	
	BE (N_1) (eV)	% (N_1)	BE (N_2) (eV)	% (N_2)	BE (N_3) (eV)	% (N_3)
BD-N-UNCD-H	398.8	15.0	401.3	73.4	403.4	11.6

Band C_1 (see also Fig. 3d in the main manuscript text), the dominant one for both the target specimens, can be ascribed to sp^3-hybridised carbon [1-4]. Under the adopted acquisition conditions (corresponding to a resolution of 0.5 eV; see the Experimental section of the main manuscript text), neither the contribution of adventitious C [2-6] nor the one of sp^2 centres, associated to defects at grain boundaries [2, 7, 8], could be resolved separately with respect to the main C_1 component.

Nonetheless, a comparison of C1s signals for samples BD-N-UNCD and BD-N-UNCD-H displayed in Fig. 3d suggested an enhanced sp^2 contribution in the latter case, as testified by

component C_3. As a matter of fact, the latter, present only for sample BD-N-UNCD-H, corresponds to a secondary *shake-up* feature typical for sp^2 C [9, 10]).

Component C_2 was assigned to C-H bonds [3, 11, 12], as well as to the concurrent contribution of C-O-C and C-OH groups [1, 3] and, for sample BD-N-UNCD-H, also to C=N and C-NH_x (x = 1, 2) groups to a minor extent [3, 4].

The attribution of O1s photopeak contributing bands (Fig. 3b in the main manuscript text) can be performed as follows: O_1, O in C-OH groups; O_2, O in C-O-C moieties [1, 13, 14]; O_3, adsorbed water due to humid air exposure prior to XPS analyses [14, 15].

As concerns the N1s signal (see also Fig. 3c in the main manuscript text), the assignment is the following: N_1, C=N-C groups [4, 6, 16]; N_2, nitrogen in NH_x groups [5, 6, 16]; N_3, "quaternary" nitrogen (analogous to graphitic N, except that, differently from with N bearing a lone-pair and singly bonded to three C, it releases one electron to form N^+ ions with four valence electrons, which can bond to three carbons in a similar fashion [10, 17]).

5. Photoelectrochemical tests

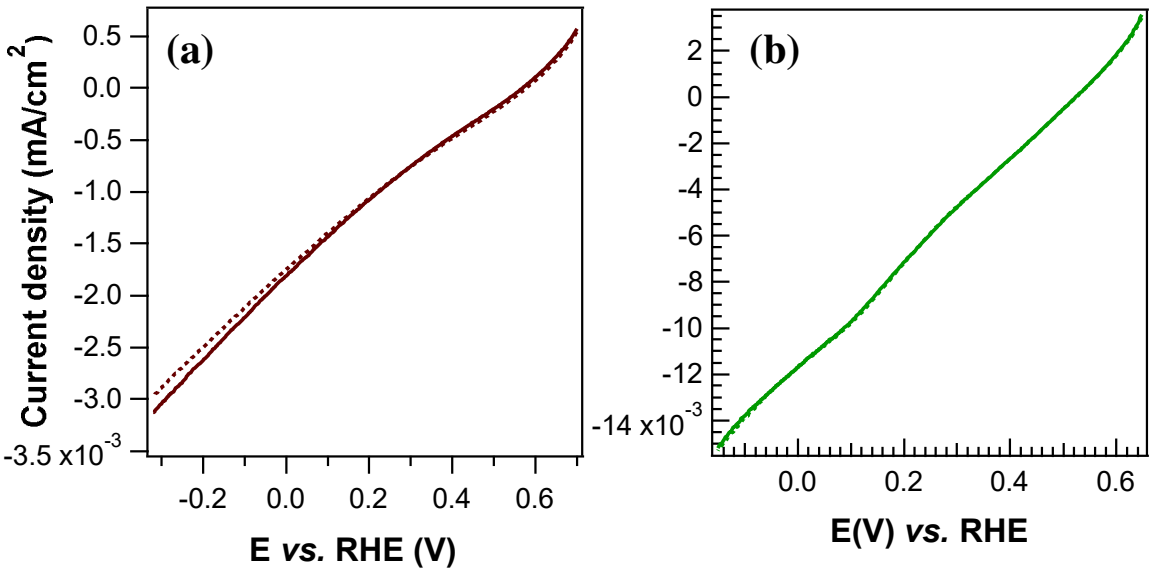

Figure S4. *LSVs collected for: (a) the BD surface; (b) the same BD surface after hydrogen plasma exposure. Dashed and continuous lines refer to dark and light conditions, respectively.*

For both the test samples, the photocurrent density shows an almost negligible variation upon illumination. This performance can be explained by the fact that the laser texturing allows Vis light absorption by the formation of defect-induced absorption centres, but hampers the exploitation of photo-generated charge carriers at the surface due to a fast surface recombination, as also explained in the main text.

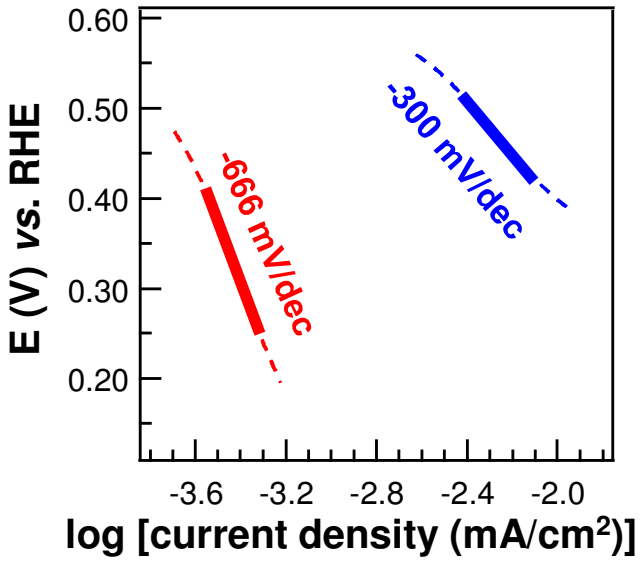

Figure S5. *Tafel plots for specimens BD-N-UNCD (red) and BD-N-UNCD-H (blue) under dark conditions. Dashed and continuous lines correspond to experimental and fitting curves, respectively.*

6. Optical analysis

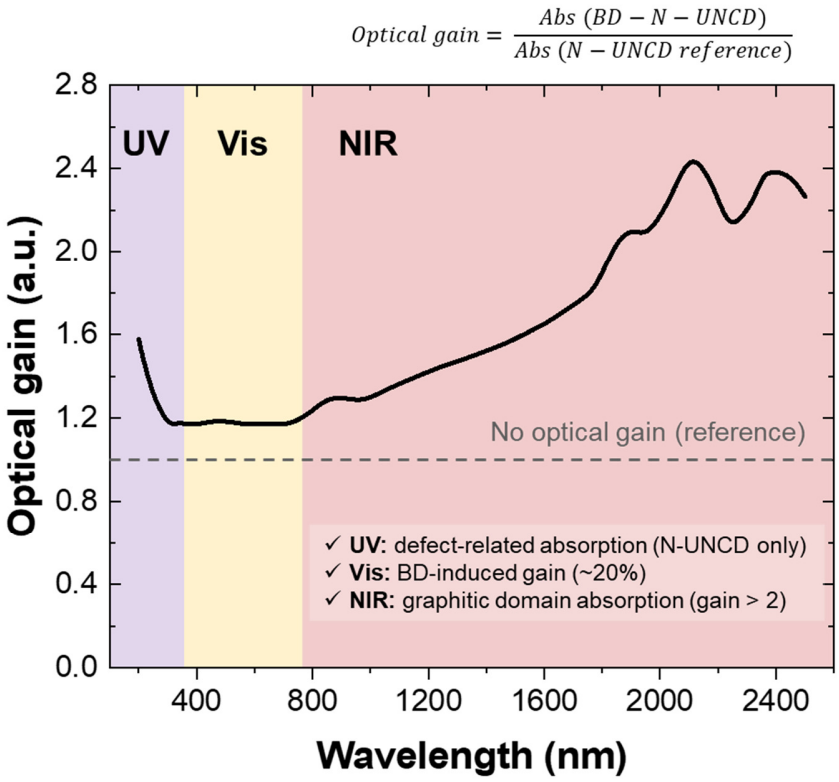

Figure S6. *Optical gain as a function of wavelength, defined as the ratio between the absorptance of the BD–N-UNCD photocathode and that of the N-UNCD reference sample, where only the N-incorporated layer was deposited without laser-induced processing. The dashed line at gain = 1 represents the condition of no enhancement.*

Fig. S6 reports the optical gain, defined as the ratio between the absorptance of the complete BD–N-UNCD photocathode and that of a reference diamond plate coated with the same N-UNCD film but without fs-laser surface nanotexturing or internal graphitic microcolumns. A gain value above unity indicates enhanced light harvesting induced by the laser-engineered BD layer.

The gain remains close to 1 in the near-UV region but rises to ≈ 1.2 across the visible band (380 – 750 nm), confirming that the surface nanotexturing reduces specular and diffuse reflectance and increases the effective optical path. In the NIR range, the gain steadily increases and exceeds 2, reflecting the strong sub-bandgap absorption arising from defect states and sp^2-bonded carbon introduced by the fs-laser treatment. These results demonstrate that the engineered BD substrate

plays an active optical role in the photocathode architecture, beyond mechanical support, by contributing significantly to Vis and NIR photon harvesting.

Table S3. *Summary of the main spectral regions relevant to the BD-N-UNCD photocathode, indicating the dominant physical absorption mechanisms and their expected contribution to the device behaviour. The table is intended to assist in interpreting the UV–Vis–NIR optical response and its correlation with the observed photo-electrocatalytic performance.*

Spectral region	Physical origin	Effect on device
300–380 nm	shallow defects + sp^2	moderate
380–750 nm	LIPSS scattering + BD defects	+20% gain
800–2000 nm	graphitic domains and deeper sub-bandgap states induced by fs-laser processing	>2× gain

To correlate the optical enhancement with the photoelectrochemical measurements performed under white LED illumination, a source-weighted absorptance was calculated. The emission spectrum of the LED source used for photoelectrochemical testing was recorded and normalized to its maximum intensity.

The source-weighted absorptance was calculated using the following equation:

$$I_{\text{abs}} = \sum_i A(\lambda_i)\, S_{\text{LED}}(\lambda_i)\, \Delta\lambda \quad \text{(S1)}$$

where $A(\lambda_i)$ is the measured absorptance (converted from % to fractional units), $S_{\text{LED}}(\lambda_i)$ is the normalized LED emission intensity, $\Delta\lambda$ = 5 nm is the spectral sampling step.

Since identical illumination conditions were applied to both samples, the relative variation of I_{abs} directly reflects the difference in effective photon harvesting.

The BD-N-UNCD structure exhibits an approximately 18% higher source-weighted absorptance compared to the reference N-UNCD configuration, in agreement with the ~20% average absorptance increase extracted from the visible spectral window (380–750 nm).

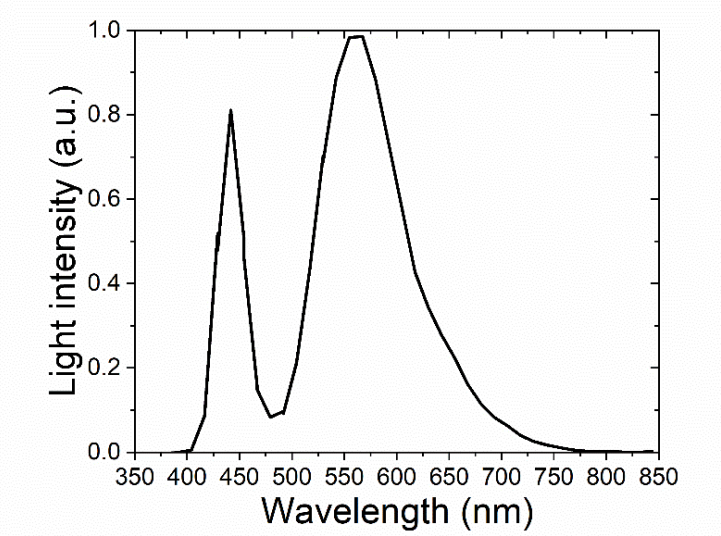

Figure S7. *Normalized emission spectrum of the white LED source (provided by Metrohm Autolab B.V.) used for the photoeletrochemical measurements. 400–800 nm is the spectral window considered for the source-weighted absorptance calculation.*

7. Work function evaluation

Table S4. *KPFM statistical analysis for the work function (φ) evaluation. The formula used for the calculation of φ is reported in the last row of the Table (see also [18]).*

Sample	CPD Average value (V_{CPD})	CPD Maximum	CPD Minimum	CPD Median
BD-N-UNCD	611.9 ± 32.6 mV	649.0 mV	583.9 mV	612.2 mV
BD-N-UNCD-H	1019.8 ± 41.9 mV	1060.2 mV	994.5mV	1019.5 mV
$\boldsymbol{\varphi = \varphi_{tip} + eV_{CPD}}$, where φ_{tip} is 4.5 ± 0.1 eV. V_{CPD} is the contact potential difference measured during KPFM tests, *e* is the electronic charge, φ_{tip} is the work function of the AFM tip.				

8. XPS valence bands

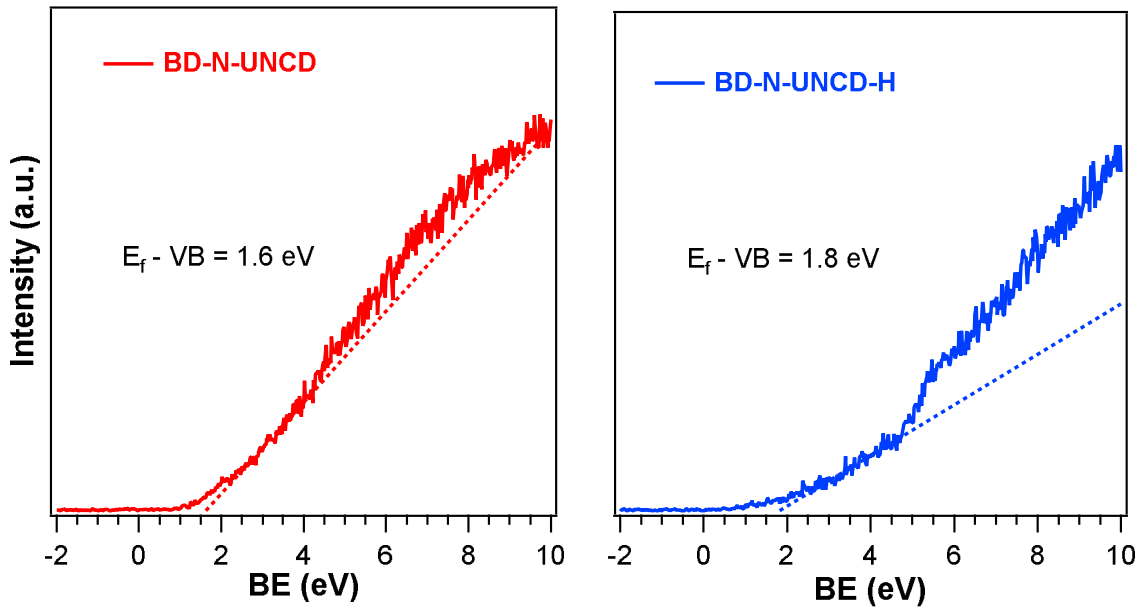

Figure S8. *XPS valence band (VB) spectra for samples BD-N-UNCD and BD-N-UNCD-H. The separation of the VB edge from the Fermi level corresponds to the interception of the linear part of the VB spectrum with the BE horizontal axis.*

9. Reflection electron energy loss spectroscopy (REELS) measurements

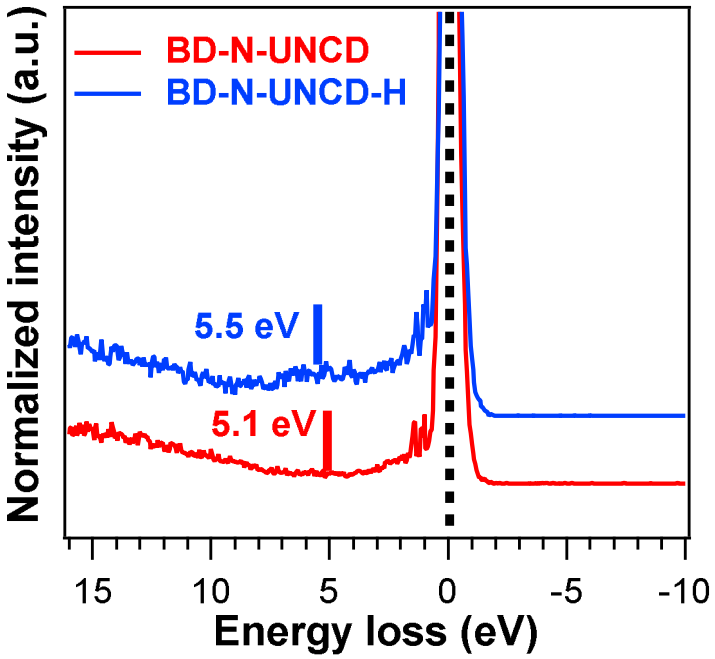

Figure S9. *REELS spectra of the two photocathodes. The extrapolated energy gap values (uncertainty = ±0.2 eV) are marked on the spectra.*

In order to avoid electron damage to material surface, REELS measurements were performed with an energy of the primary electron beam of 1 keV [12]. As-recorded REELS spectra for the two samples are plotted in Fig. S9 without elastic peak subtraction.

The recorded spectra were characterized by an intense peak at zero energy loss due to elastically scattered electrons, and signals below 2 eV due to scattering collisions with hydrogen atoms [19, 20]. In particular, the peaks at ≈ 1 and 1.5 eV are typical of C-H wagging and stretching vibrations, respectively. It is worthwhile noticing that BD-N-UNCD-H showed a broad feature centered at ≈ 5 eV due to the collective excitation of π electrons [20]. This is in line with the increased content of sp^2 defects, as discussed in relation to XPS data.

10. Additional electrochemical data

Table S5. *Representative photoelectrochemical performances of diamond-based selected electrodes. BDD = Boron Doped Diamond; (a) Overpotential = 1.25 V; (b)NiO = 15 foils; (c) Mercury lamp; (d) 1 sun (100 mW/cm^2); (e) HgXe light source with UV cutoff filter; (f) White LED source (400-800 nm, 100 mW/cm^2). N.A. = not available.*

Material	Intrinsic film (10-20 µm) on W	BDD on W	Pt-decorated BDD	NiO - Cu_2O/BDD *(b)*	DND on BDD	NDD on BDD	**BD-N-UNCD-H**
j @ 0.0 V vs RHE	-10 µA/cm^2	0.01 µA/cm^2 *(a)*	-	-0.42 mA/cm^2	≈ -0.008 mA/cm^2	≈ -0.01 mA/cm^2	-0.13 mA/cm^2
Reaction medium	1M KCl	0.5 M H_2SO_4	H_2 saturated 0.1 M H_2SO_4	0.1 M Na_2SO_4	0.1 M KCl	0.1 M KCl	0.1 M Na_2SO_4
Use of light	Yes *(c)*	No	No	Yes *(d)*	Yes *(e)*	Yes *(e)*	Yes *(f)*
Tafel slope	N.A.	197 mV/dec	N.A.	N.A.	1475 mV/dec	536 mV/dec	273 mV/dec
Reference	[21]	[22]	[23]	[24]	[25]	[25]	[This work]

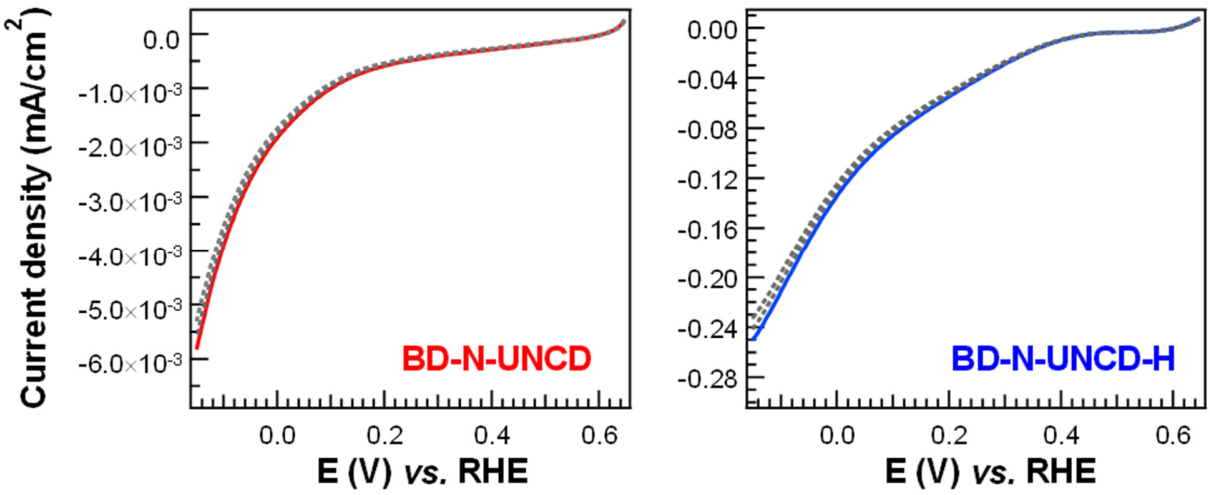

Figure S10. *LSV curves recorded under illumination on the samples for the first measurements (solid lines) and every 90 days over a period of six months (grey lines).*

11. XPS characterization after electrochemical tests

Table S6. *Atomic percentages for the specimens under investigation before and after electrochemical tests indicated in the caption of Fig. S10.*

Sample	C (at.%)	O (at.%)	N (at.%)
BD-N-UNCD	98.7	1.3	---
BD-N-UNCD post-EC	85.3	14.7	---
BD-N-UNCD-H	94.4	4.8	0.8
BD-N-UNCD-H post-EC	85.9	12.6	1.5

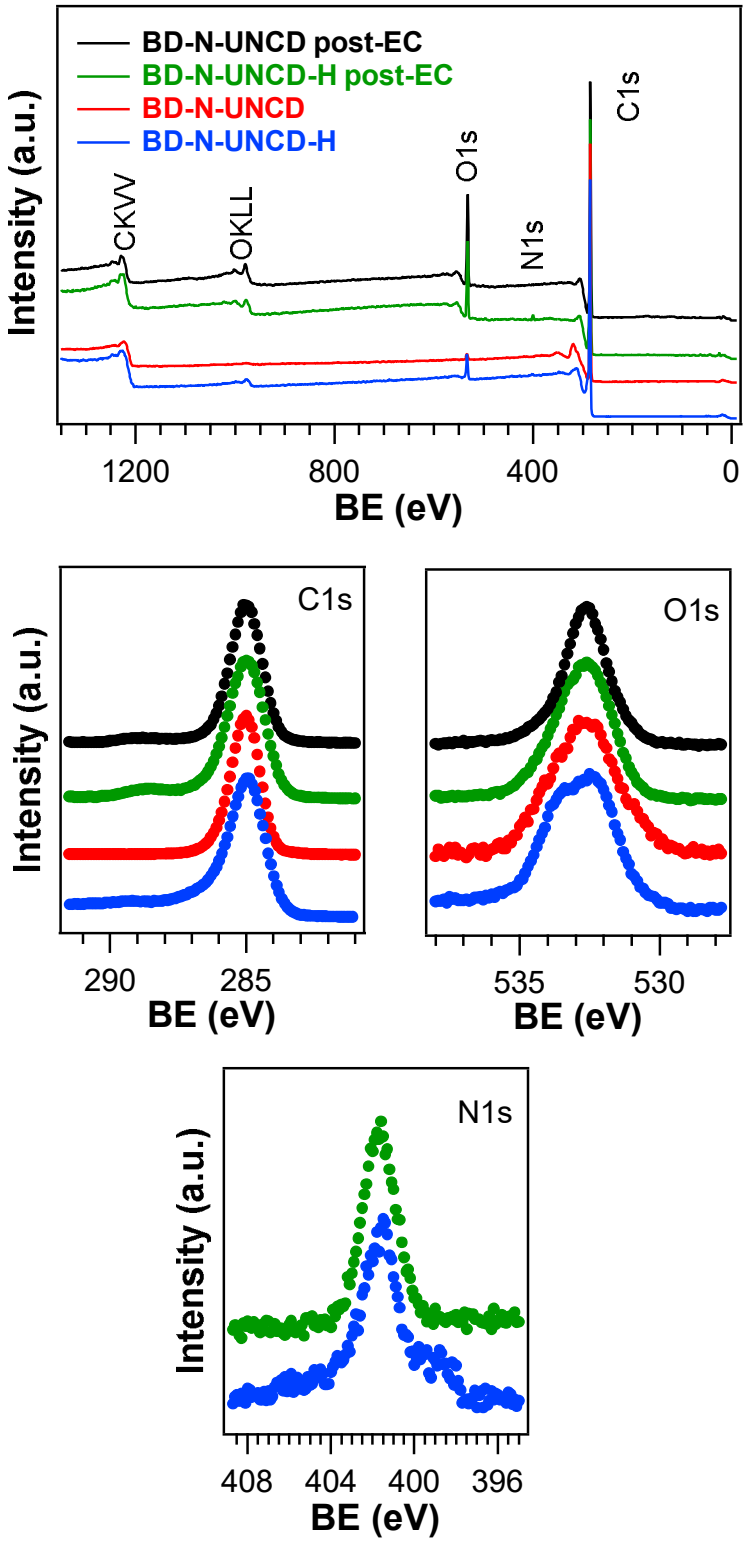

Figure S11. *XPS analyses before and after (indicated in the caption as post-EC) completion of electrochemical tests indicated in the caption of Fig. S10 for the target samples: wide-scan spectra; C1s, O1s, and N1s photoelectron peaks.*

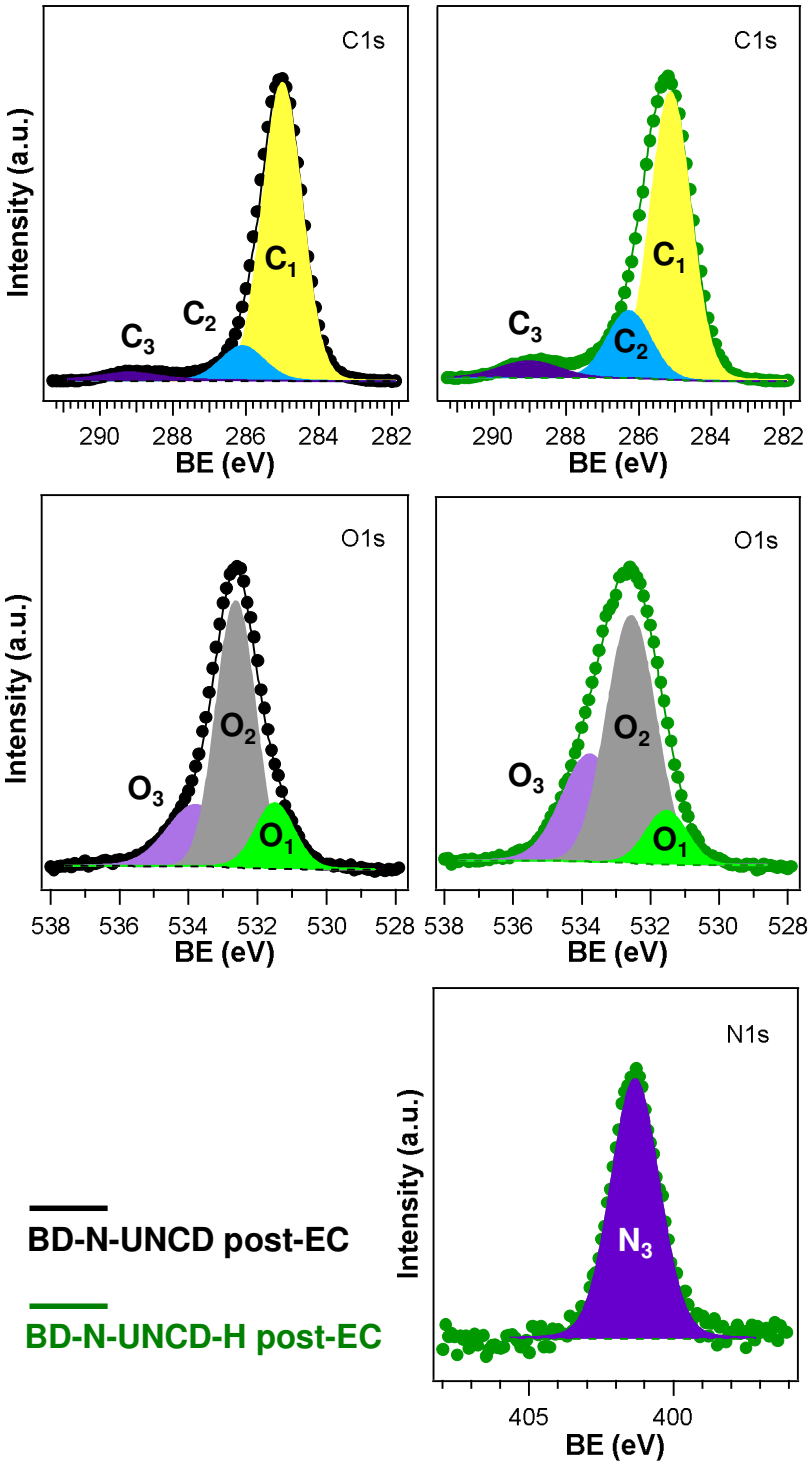

Figure S12. *C1s, O1s and N1s photoelectron peaks, along with pertaining fittings, after completion of electrochemical tests indicated in the caption of Fig. S10 for BD-N-UNCD and BD-N-UNCD-H samples.*

Table S7. *XPS results: binding energy (BE) and contributions (%) of the various bands for the overall C1s, O1s and N1s peaks after completion of electrochemical tests indicated in the caption of Fig. S10.*

Sample	C_1		C_2		C_3	
	BE (C_1) (eV)	% (C_1)	BE (C_2) (eV)	% (C_2)	BE (C_3) (eV)	% (C_3)
BD-N-UNCD post-EC	285.0	83.7	286.1	11.3	289.2	5.0
BD-N-UNCD-H -post-EC	285.0	75.2	286.2	18.6	289.1	4.5
Sample	O_1		O_2		O_3	
	BE (O_2) (eV)	% (O_2)	BE (O_3) (eV)	% (O_3)	BE (O_4) (eV)	% (O_4)
BD-N-UNCD post-EC	531.5	16.0	532.6	61.8	533.8	22.2
BD-N-UNCD-H -post-EC	531.5	10.8	532.6	58.8	533.8	34.0
Sample	N_1		N_2		N_3	
	BE (N_1) (eV)	% (N_1)	BE (N_2) (eV)	% (N_2)	BE (N_3) (eV)	% (N_3)
BD-N-UNCD-H -post-EC	---	---	401.3	100.0	---	---

12. References

[1] R. Zulkharnay, G. Zulpukarova, P.W. May, Oxygen-terminated diamond: insights into the correlation between surface oxygen configurations and work function values, Appl. Surf. Sci., 658 (2024) 159776.

[2] T. Haensel, J. Uhlig, R.J. Koch, S.I.-U. Ahmed, J.A. Garrido, D. Steinmüller-Nethl, M. Stutzmann, J.A. Schaefer, Influence of hydrogen on nanocrystalline diamond surfaces investigated with HREELS and XPS, Phys. Status Solidi A, 206 (2009) 2022-2027.

[3] A. Chemin, M.K. Kuntumalla, M. Brzhezinskaya, T. Petit, A. Hoffman, Depth profiling of microwave nitrogen-terminated polycrystalline diamond surfaces by energy-dependent X-ray photoelectron spectroscopy, Appl. Surf. Sci., 661 (2024) 160082.

[4] R. Malkinson, M.K. Kuntumalla, A. Chemin, T. Petit, A. Hoffman, N. Bar-Gill, Enhanced quantum properties of shallow diamond atomic defects through nitrogen surface termination, J. Mater. Chem. C, 12 (2024) 7206-7213.

[5] E. Scattolin, M. Benedet, D. Barreca, G.A. Rizzi, A. Gasparotto, C. Maccato, Graphitic carbon nitride functionalized with NiO nanoaggregates: An X-ray photoelectron spectroscopy investigation, Surf. Sci. Spectra, 31 (2024) 024001.

[6] G. Marchiori, M. Brugia, T. Sturaro, M. Benedet, D. Barreca, A. Gasparotto, G.A. Rizzi, C. Maccato, ZnO and $ZnFe_2O_4$-functionalized graphitic carbon nitride: An XPS study, Surf. Sci. Spectra, 32 (2025) 014003.

[7] B. Lesiak, L. Kövér, J. Tóth, J. Zemek, P. Jiricek, A. Kromka, N. Rangam, C sp^2/sp^3 hybridisations in carbon nanomaterials – XPS and (X)AES study, Appl. Surf. Sci., 452 (2018) 223-231.

[8] J.C. Arnault, S. Saada, O.A. Williams, K. Haenen, P. Bergonzo, M. Nesladek, R. Polini, E. Osawa, Surface characterisation of silicon substrates seeded with diamond nanoparticles under UHV annealing, Phys. Status Solidi A, 205 (2008) 2108-2113.

[9] A. Theodosiou, B.F. Spencer, J. Counsell, A.N. Jones, An XPS/UPS study of the surface/near-surface bonding in nuclear grade graphites: A comparison of monatomic and cluster depth-profiling techniques, Appl. Surf. Sci., 508 (2020) 144764.

[10] G. Marchiori, M. Benedet, A. Fasan, D. Barreca, C. Maccato, G.A. Rizzi, A. Gasparotto, XPS investigation of Cu_xO-functionalized amorphous carbon nitride, Surf. Sci. Spectra, 31 (2024) 024010.
[11] M.K. Kuntumalla, A. Chemin, N. Matos Doron, M. Brzhezinskaya, T. Petit, A. Hoffman, Impact of acid etching on surfaces and near-surface region in nitrogen plasma terminated polycrystalline diamond, Diam. Relat. Mater., 158 (2025) 112623.
[12] M.K. Kuntumalla, S. Michaelson, A. Hoffman, Nitrogen, oxygen, and hydrogen bonding and thermal stability of ambient exposed nitrogen-terminated H-diamond (111) surfaces studied by XPS and HREELS, Surf. Sci., 749 (2024) 122555.
[13] I. Bertóti, M. Mohai, K. László, Surface modification of graphene and graphite by nitrogen plasma: Determination of chemical state alterations and assignments by quantitative X-ray photoelectron spectroscopy, Carbon, 84 (2015) 185-196.
[14] R. Akhvlediani, S. Michaelson, A. Hoffman, Interaction of water molecules with bare and deuterated polycrystalline diamond surface studied by high resolution electron energy loss and X-ray photoelectron spectroscopies, Surf. Sci., 604 (2010) 2129-2138.
[15] M.A. Henderson, The interaction of water with solid surfaces: fundamental aspects revisited, Surf. Sci. Rep., 46 (2002) 1-308.
[16] M. Benedet, A. Gasparotto, G.A. Rizzi, D. Barreca, C. Maccato, g-C3N4-based materials functionalized with Au, Ag, and Au-Ag: An XPS study, Surf. Sci. Spectra, 29 (2022).
[17] N. Hellgren, R.T. Haasch, S. Schmidt, L. Hultman, I. Petrov, Interpretation of X-ray photoelectron spectra of carbon-nitride thin films: New insights from in situ XPS, Carbon, 108 (2016) 242-252.
[18] R. Salerno, V. Valentini, E. Bolli, M. Mastellone, V. Serpente, A. Mezzi, L. Tortora, E. Colantoni, A. Bellucci, R. Polini, D.M. Trucchi, Low Electron Affinity Silicon/Nanocrystalline Diamond Heterostructures for Photon-Enhanced Thermionic Emission, ACS Appl. Energy Mater., 7 (2024) 868-873.
[19] M. Benedet, A. Fasan, D. Barreca, C. Maccato, C. Sada, S.M. Deambrosis, V. Zin, F. Montagner, O.I. Lebedev, E. Modin, G.A. Rizzi, A. Gasparotto, Plasma-assisted fabrication of ultra-dispersed copper oxides in and on C-rich carbon nitride as functional composites for the oxygen evolution reaction, Dalton Trans., 53 (2024) 17452-17464.

[20] S.D. Nehate, A.K. Saikumar, K.B. Sundaram, Influence of Substrate Temperature on Electrical and Optical Properties of Hydrogenated Boron Carbide Thin Films Deposited by RF Sputtering, Coatings, 11 (2021) 196.
[21] Y.V. Pelskov, A.Y. Sakharova, M.D. Krotova, L.L. Bouilov, B.V. Spitsyn, Photoelectrochemical properties of semiconductor diamond, J. Electroanal. Chem. 228 (1987) 19-27.
[22] H.B. Martin, A. Argoitia, U. Landau, A.B. Anderson, J.C. Angus, Hydrogen and Oxygen Evolution on Boron-Doped Diamond Electrodes, J. Electrochem. Soc., 143 (1996) L133.
[23] T. Brulle, A. Denisenko, H. Sternschulte, U. Stimming, Catalytic activity of platinum nanoparticles on highly boron-doped and 100-oriented epitaxial diamond towards HER and HOR, Phys. Chem. Chem. Phys., 13 (2011) 12883-12891.
[24] C.K. Mavrokefalos, M. Hasan, J.F. Rohan, R.G. Compton, J.S. Foord, Electrochemically deposited Cu_2O cubic particles on boron doped diamond substrate as efficient photocathode for solar hydrogen generation, Appl. Surf. Sci., 408 (2017) 125-134.
[25] T. Yoshikawa, A. Kaga, K. Ichikawa, K. Hayashi, T. Matsumoto, R. Izumi, M. Ohno, S. Yamasaki, N. Tokuda, H. Asakawa, Enhanced performance of diamond electrodes with heavily N-doped surface nanolayers grown by CVD for high reduction current density, Electrochim. Acta, 525 (2025).